Article

Capsaicin restores sodium iodine symporter-mediated radioiodine uptake through bypassing canonical TSH–TSHR pathway in anaplastic thyroid carcinoma cells

Shichen Xu[1], Xian Cheng[1], Jing Wu[1], Yunping Wang[2], Xiaowen Wang[2], Liying Wu[2], Huixin Yu[1], Jiandong Bao[1], and Li Zhang[1,3,4,*]

[1] NHC Key Laboratory of Nuclear Medicine, Jiangsu Key Laboratory of Molecular Nuclear Medicine, Jiangsu Institute of Nuclear Medicine, Wuxi 214063, China
[2] School of Food Science and Technology, Jiangnan University, Wuxi 214122, China
[3] Department of Radiopharmaceuticals, School of Pharmacy, Nanjing Medical University, Nanjing 211166, China
[4] School of Life Science and Technology, Southeast University, Nanjing 210096, China
* Correspondence to: Li Zhang, E-mail: zhangli@jsinm.org

Edited by Zhiyuan Shen

Anaplastic thyroid cancer (ATC) is a rare but highly lethal disease. ATCs are resistant to standard therapies and are extremely difficult to manage. The stepwise cell dedifferentiation results in the impairment of the iodine-metabolizing machinery and the infeasibility of radioiodine treatment in ATC. Hence, reinducing iodine-metabolizing gene expression to restore radioiodine avidity is considered as a promising strategy to fight against ATC. In the present study, capsaicin (CAP), a natural potent transient receptor potential vanilloid type 1 (TRPV1) agonist, was discovered to reinduce ATC cell differentiation and to increase the expression of thyroid transcription factors (TTFs including TTF-1, TTF-2, and PAX8) and iodine-metabolizing proteins, including thyroid-stimulating hormone receptor (TSHR), thyroid peroxidase, and sodium iodine symporter (NIS), in two ATC cell lines, 8505C and FRO. Strikingly, CAP treatment promoted NIS glycosylation and its membrane trafficking, resulting in a significant enhancement of radioiodine uptake of ATC cells *in vitro*. Mechanistically, CAP-activated TRPV1 channel and subsequently triggered Ca^{2+} influx, cyclic adenosine monophosphate (cAMP) generation, and cAMP-responsive element-binding protein (CREB) signal activation. Next, CREB recognized and bound to the promoter of *SLC5A5* to facilitate its transcription. Moreover, the TRPV1 antagonist CPZ, the calcium chelator BAPTA, and the PKA inhibitor H-89 effectively alleviated the redifferentiation exerted by CAP, demonstrating that CAP might improve radioiodine avidity through the activation of the TRPV1–Ca^{2+}/cAMP/PKA/CREB signaling pathway. In addition, our study indicated that CAP might trigger a novel cascade to redifferentiate ATC cells and provide unprecedented opportunities for radioiodine therapy in ATC, bypassing canonical TSH–TSHR pathway.

Introduction

Thyroid cancer is the most common endocrine malignancy with a substantial global rise in incidence (Kim et al., 2020). According to the histological classification, follicular thyroid cell-derived tumors can be classified into papillary thyroid carcinoma (PTC), follicular thyroid carcinoma (FTC), poorly differentiated thyroid carcinoma (PDTC), and anaplastic thyroid carcinoma (ATC) (Xing, 2013). Although rare, ATC is almost invariably associated with increased incurability and patient mortality, with a median survival time ∼5 months (Maniakas et al., 2020). Even worse, conventional therapies, including surgery, thyroid-stimulating hormone (TSH) suppression, radiotherapy, and chemotherapy, have almost no efficiency against ATC, mainly because of a progressive dedifferentiation status of ATC (Nikiforov

and Nikiforova, 2011). Accompanied by the process of stepwise dedifferentiation, ATC cells are going to lose the biological characteristics or functions of normal follicular thyroid cells, such as the expression of thyroid-associated transcription factors (TTFs) and iodine-metabolizing genes, TSH-dependent iodine uptake, and thyroid hormone synthesis (Xing, 2013).

As known, thyroid hormone synthesis using iodine is a primary and unique function of follicular thyroid cells (Xing, 2013). In such process, iodine is transported into the cell through sodium iodine symporter (NIS), which is located on the basolateral membrane. At the apical membrane, pendrin transports iodine out of the cell into the thyroid lumen, where it is organified by thyroid peroxidase (TPO) and incorporated into the tyrosine residues in thyroglobulin (TG) to produce thyroid hormone. Basically, this process can be precisely regulated by cyclic adenosine monophosphate (cAMP) signaling that is triggered by TSH-mediated activation of thyroid-stimulating hormone receptor (TSHR) (Xing, 2013). Therefore, radioiodine therapy against thyroid cancer is based on the active transport of iodine through plasma membrane-expressed NIS. However, loss of expression of these thyroid iodine-metabolizing genes is one of the hallmarks of advanced thyroid cancers. It is believed that the decreased or absent expression of NIS directly results in the failure of radioiodine treatment for the patients who are usually refractory to radioiodine therapy (Landa et al., 2016).

Many strategies have been proposed to induce redifferentiation of ATC cells for the restoration of radioiodine avidity (Buffet et al., 2020), and these attempts are primarily based on upregulating NIS expression (Xing, 2013). It has been reported that the MAPK pathway is frequently activated during thyroid tumorigenesis and associated with the NIS repression. Therefore, targeting MAPK using tyrosine kinase inhibitors emerged as one of the most promising therapeutic modalities. For instance, several latest studies have demonstrated that targeting BRAF V600E, the most common oncogenic mutation in thyroid cancer (Xing, 2005), by vemurafenib could reinduce thyroid functional gene expression and radioiodine uptake in thyroid cancer cells (Cheng et al., 2016; Zhang and Chen, 2018). In addition, vemurafenib was discovered to restore radioiodine uptake and efficacy in a subset of BRAF-mutant radioiodine-refractory thyroid cancer patients in clinic trial (Dunn et al., 2019). It has been reported that targeting the PI3K/AKT/mTOR or Notch pathway could also significantly increase NIS protein level along with the augmented radioiodine avidity (Hou et al., 2010; Yu et al., 2013). In addition to modulating crucial signaling pathways involved in thyroid cancer dedifferentiation, multiple promising therapies and agents such as epigenetic modulators (Zhu et al., 2017), post-transcriptional (Wachter et al., 2018) and post-translational (Smith et al., 2011) regulators, and immunotherapy (Ma et al., 2020) are thoroughly investigated in preclinical and clinical trials. Molecular profiling of ATCs is increasingly used to search for therapeutic targets that may inform individualized targeted therapy. A Phase 2 clinical trial with dabrafenib (BRAF inhibitor) plus trametinib (MEK inhibitor) showed a significant response rate in ATC patients with the BRAF V600E mutation. The combination is now approved by the US Food and Drug Administration for this indication (Bible et al., 2021). Although lots of promising treatment modalities emerge, novel therapeutic strategies for ATC are still desperately needed.

Capsaicin (CAP) is a transient receptor potential vanilloid type 1 (TRPV1) agonist, which was discovered to be a potent anticancer agent against several types of cancer (Clark and Lee, 2016). Consistently, our previous study proved that CAP could inhibit the metastasis of human PTC cells through TRPV1 channel *in vitro* (Xu et al., 2018). It is worth noting that when TRPV1 is activated by CAP, calcium, a ubiquitous cellular second messenger, enters into the cell and ultimately results in disturbance of intracellular calcium homeostasis (Diaz-Laviada and Rodriguez-Henche, 2014). It is believed that Ca^{2+} signal is closely involved in tumorigenesis and tumor progression (Zhong et al., 2019). Hence, Ca^{2+} modulation is expected to be a novel pharmacological and therapeutic target in cancer treatment. Our recent study demonstrated that CAP induced mitochondrial dysfunction and apoptosis in ATC cells via TRPV1-mediated mitochondrial calcium overload (Xu et al., 2020a). Besides, there is a close relationship between intracellular calcium signal and cAMP generation. It has been reported that calcium entry activates soluble adenylyl cyclase, causing an increase in cAMP (Tanzarella et al., 2019). Hence, the distinct characteristics of CAP prompted us to investigate whether CAP could activate cAMP and regulate iodine-metabolizing gene expression through increasing intracellular calcium.

In the present study, we reported that CAP treatment may serve as a potential therapeutic strategy for radioactive iodine-refractory differentiated thyroid cancer (RAIR-DTC)/ATC by restoring NIS expression and iodine avidity, mainly through bypassing TSH−TSHR machinery but activating the TRPV1−Ca^{2+}/cAMP/protein kinase A (PKA)/cAMP-responsive element-binding protein (CREB) signaling pathway.

Results

The expression levels of both TTFs and iodine-metabolizing genes are downregulated in ATCs

The accumulation of genetic alterations during thyroid tumorigenesis serves as one of the driving factors for differentiated thyroid carcinoma (PTC and FTC) to progress to PDTC or even to ATC, which is the most aggressive thyroid cancer (Xing, 2013). In the process of stepwise dedifferentiation, aberrant silence of thyroid iodine-metabolizing genes is responsible for the loss of radioiodine avidity and consequent failure of radioiodine treatment for thyroid cancers. In the present study, we first performed a bioinformatics analysis based on a combined Gene Expression Omnibus (GEO) cohort of thyroid cancers (GSE29265, GSE35570, GSE76039, GSE65144, GSE82208, and GSE53157) to investigate the expression levels of iodine-metabolizing genes across different types of thyroid cancers. The combined GEO cohort included 81 nontumoral/normal thyroid tissues, 78 PTCs, 31 FTCs, 22 PDTC, and 52 ATCs.
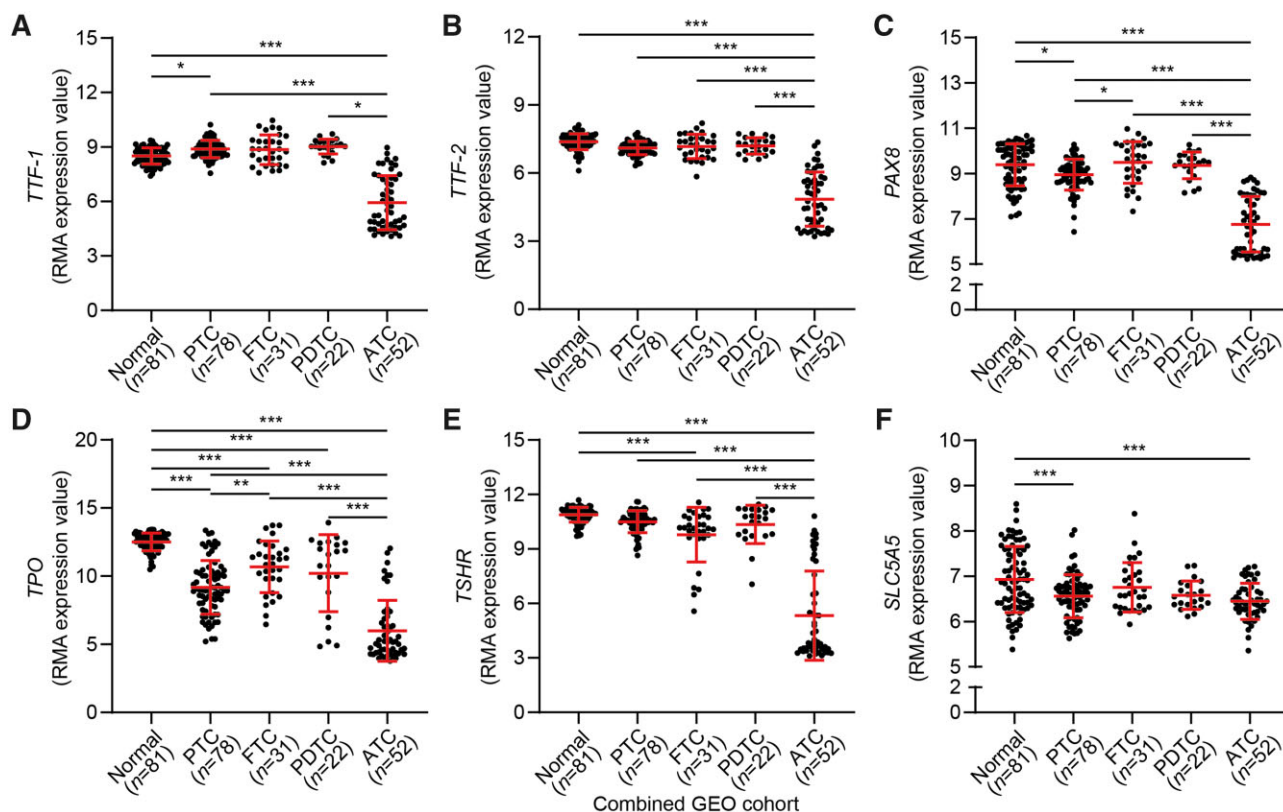
Figure 1 Bioinformatics analysis of TTFs and thyroid iodine-metabolizing genes in the combined GEO cohort of thyroid cancers. (A–F) Robust RMA expression values of *TTF-1* (**A**), *TTF-2* (**B**), *PAX8* (**C**), *TPO* (**D**), *TSHR* (**E**), and *SLC5A5* (**F**) were compared among normal thyroid tissues, PTCs, FTCs, PDTCs, and ATCs in the combined GEO cohort. *$P < 0.05$, **$P < 0.01$, ***$P < 0.001$, one-way ANOVA.

As shown in Figure 1, in accordance with the stepwise dedifferentiation from well-differentiated PTC to ATC, the expression levels of TTFs (*TTF-1*, *TTF-2*, and *Pax8*) and thyroid-specific functional genes (*TPO*, *TSHR*, and *SLC5A5*, which encodes NIS) gradually reduced along the spectrum of disease progression. As expected, ATCs had the lowest expression levels of these thyroid functionally related genes among all types of thyroid cancers. More importantly, *SLC5A5*, which is directly responsible for iodine uptake of thyroid follicular cells, significantly decreased in ATCs compared with normal tissues. As known, the process of iodine uptake is upregulated by TSH–TSHR stimulation (Xing, 2013). However, we observed that TSHR expression was also dramatically declined in ATCs (Figure 1E). Hence, the biological basis for the conventional radioiodine treatment of thyroid cancer was notably impaired in ATCs, resulting in the infeasibility of radioiodine therapy in ATCs.

CAP restores thyroid-specific gene expression and enhances radioiodine uptake of ATC cells

Simultaneous and abundant expression of TTFs, such as TTF-1, TTF-2, and PAX8, is essential for the development, survival, differentiation, and proper physiological functions of thyroid follicular cells (Kambe and Seo, 1997). Besides, TTF-1, TTF-2, and PAX8 can bind to the promoters of *SLC5A5*, *TG*, and *TPO* genes, and TTF-1

can also bind to the enhancer and promoter of *TSHR* (Christophe-Hobertus et al., 2012). Thus, the coordinated expression of TTFs is essential for maintaining the function of the differentiated thyroid (Fernández et al., 2015). Interestingly, we found that CAP, a potent TRPV1 agonist, increased the mRNA expression levels of *TTF-2* and *PAX8* to a certain degree but downregulated *TTF-1* expression significantly in 8505C cells, a commonly used ATC cell line. Meanwhile, CAP could simultaneously increase the mRNA expression levels of iodine-metabolizing genes including *NIS*, *TSHR*, and *TPO* to some extent in a dose-dependent manner. Notably, *NIS* mRNA expression was dramatically upregulated after 200 µM CAP treatment, evidenced by quantitative real-time polymerase chain reaction (qPCR) (Figure 2A). Instead, CAP treatment dose-dependently increased TTF-1 expression at the protein level (Figure 2B). Thus, a cycloheximide (CHX) chase assay was performed to determine whether CAP could enhance the protein stability of TTF-1. As shown in Figure 2C, CAP-treated cells showed a longer half-life of TTF-1 (3.9 h) compared to that of untreated control cells (0.68 h). These results demonstrated that CAP regulated TTFs not only at translational but also at post-translational levels.

In the process of thyroid hormone biosynthesis, iodine is transported into thyroid follicular cells through NIS, which is located on the basal membrane (Xing, 2013). Hence, adequate expression and membrane-targeting of NIS are indispensable for effective radioactive iodine therapy for thyroid cancer. NIS
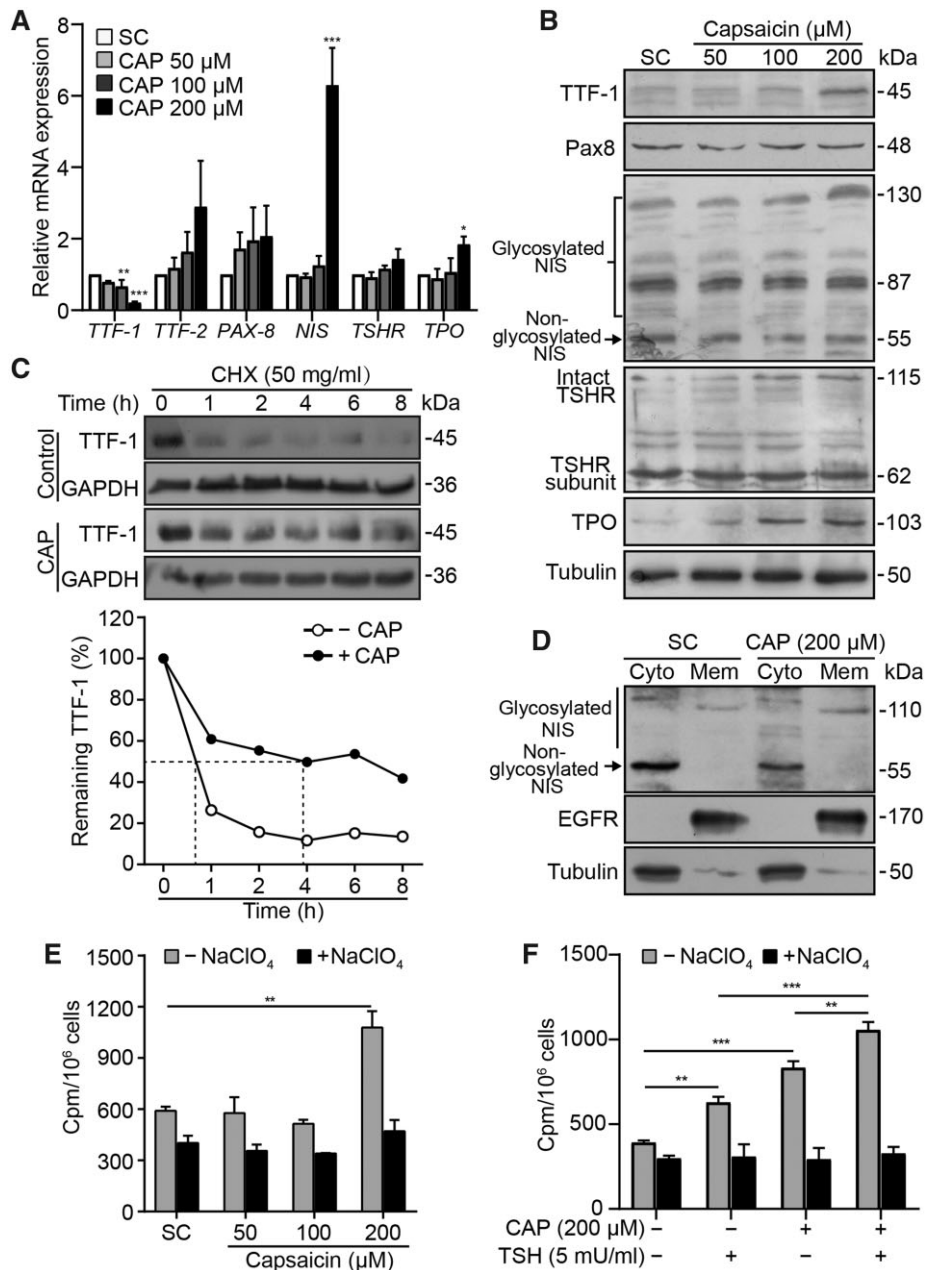
Figure 2 CAP restores thyroid-specific gene expression and enhances radioiodine uptake of ATC cells. (**A**) 8505C cells were incubated with CAP (50–200 μM) for 24 h and then the mRNA levels of *TTF-1*, *TTF-2*, *PAX8*, *NIS*, *TSHR*, and *TPO* were analyzed by qPCR. *$P < 0.05$, **$P < 0.01$, ***$P < 0.001$ vs. SC, one-way ANOVA. (**B**) 8505C cells were treated with different concentrations of CAP (50–200 μM) for 24 h and then the protein levels of TTF-1, PAX8, NIS, TSHR, and TPO were analyzed by western blotting. Tubulin was used as an internal loading control. (**C**) 8505C cells were pretreated with CAP (200 μM) for 24 h followed by CHX (50 μg/ml) treatment for the indicated periods of time. Whole-cell lysate was extracted at each time point and immunoblotted with anti-TTF-1 or GAPDH antibody. GAPDH was used as a loading control. The protein bands were quantified by optical densitometry using ImageJ software, and the remaining protein levels of TTF-1 were plotted against time points. (**D**) After 8505C cells were treated with CAP for 24 h, the membranal and cytoplasmic proteins were extracted, respectively. The subcellular localization of NIS on membrane or cytoplasm was detected by western blotting. EGFR and tubulin served as membranal (Mem) and cytoplasmic (Cyto) loading controls, respectively. (**E**) 8505C cells were pretreated with CAP (50–200 μM) for 24 h, followed by incubation with 37 kBq Na[131]I for additional 1 h in the presence or absence of 100 μM NaClO$_4$. After three times of wash by ice-cold PBS, the radioactive iodine accumulated in 8505C cells was measured using a gamma-counter. **$P < 0.01$ vs. SC, one-way ANOVA. (**F**) 8505C cells were treated with the vehicle (DMSO), CAP (200 μM), rTSH (5 mU/ml), or CAP (200 μM) in combination with rTSH (5 mU/ml) for 24 h in the presence or absence of 100 μM NaClO$_4$, and then the radioiodine uptake of cells was detected. **$P < 0.01$, ***$P < 0.001$, one-way ANOVA. The data shown represent mean ± SEM of three independent experiments ($n = 3$).

is first synthesized as a precursor of $\sim$56 kDa and then gradually matured by endoplasmic reticulum–Golgi glycosylation (Dohan et al., 2003). After CAP treatment, the amount of mature hyper-glycosylated-NIS protein with molecular weight >100 kDa increased in ATC 8505C cells, whereas the protein level of precursor NIS ($\sim$55 kDa) remained unchanged (Figure 2B). Similar results were obtained in another ATC cell line, FRO (Supplementary Figure S1). Moreover, the membranal and cytoplasmic cell fractions were separated and analyzed. Treatment of 8505C cells with CAP (200 μM) resulted in a decrease of precursor NIS protein in cytoplasm. Meanwhile, mature NIS protein was accumulated on the cell membrane of CAP-treated cells, which was twice as much as that of untreated control cells (Figure 2D). These results indicated that CAP could promote NIS glycosylation and enhance the membrane trafficking of NIS. TSHR is a member of G-protein-coupled receptors containing two subunits. Subunit A constitutes a large extracellular domain, while subunit B is a transmembrane and intracellular domain (Davies et al., 2005). When TSH interacts with TSHR, the activated TSHR increases biosynthesis of NIS through activating the cAMP system and stimulates I$^-$ accumulation (Kogai et al., 1997). Moreover, in the process of thyroid hormone synthesis, iodine undergoes oxidation by TPO (Xing, 2013). As shown in Figure 2B, CAP treatment increased the protein levels of intact TSHR and TPO as well in 8505C cells.

Considering that CAP partially restored the expression of thyroid functionally related proteins in ATC cells, we next investigated whether CAP could increase cellular radioiodine uptake. As shown in Figure 2E, 200 μM CAP treatment significantly promoted ^{131}I uptake of 8505C cells. Of note, the cellular uptake of ^{131}I sharply diminished after sodium perchlorate (NaClO$_4$, an NIS antagonist) treatment (Josefsson et al., 2006), which indicated that CAP-induced cellular ^{131}I uptake was specifically mediated by the transporter NIS. As known, TSH-mediated activation of TSHR facilitates thyroid follicular cells to synthesize thyroid hormone by absorbing iodine (Xing, 2013). As expected, we observed that the uptake of ^{131}I in 8505C cells was significantly increased after recombinant human TSH (rTSH) stimulation. In addition, ^{131}I uptake was further enhanced by the combination treatment of rTSH and CAP (Figure 2F). Collectively, these results suggested that CAP could reinduce the expression of iodine-metabolizing genes and, more importantly, enhanced ^{131}I uptake in ATC cells.

TRPV1 expression is upregulated in thyroid cancers

CAP performs its pharmacological activities mainly by TRPV1 channel, which is a nonselective cation channel (Caterina et al., 1997). Next, we analyzed TRPV1 expression levels in both the PTC/RAIR-DTC cohort of Jiangyuan Hospital and two other public databases. The cohort of Jiangyuan Hospital contained 32 well-differentiated PTC patients, who had no clinical indications for radioiodine therapy, and 21 RAIR-DTC/PDTC patients, who had experienced repeated radioiodine treatments (detailed clinical characteristics of these RAIR-DTC patients in Supplementary Table S1). It should be noted that, because of the scarcity of ATC patient samples, the analysis of TRPV1 expression was only performed in a PTC/RAIR-DTC cohort of Jiangyuan Hospital. The results obtained from immunohistochemistry (IHC) staining confirmed that the expression levels of NIS and TSHR showed a decline tendency in RAIR-DTCs compared to PTCs. However, TRPV1 expression showed a slightly increase (Figure 3A and B). Consistently, western blotting analysis of 12 PTCs also demonstrated that the expression of TRPV1 was upregulated in PTCs compared to the matched noncancerous tissues. We found that most of PTCs showed a decrease in the expression levels of NIS and TSHR (Figure 3C; Supplementary Figure S2 and Table S2). It is believed that PDTCs and ATCs shared many common characteristics and both of them were thought to arise from preexisting PTCs, where they consistently shared similar driver mutations and dedifferentiation status (Landa et al., 2016). Hence, it is reasonable for us to speculate that TRPV1 expression level also increased in ATCs. Consistent with our experimental results, the bioinformatics analysis data obtained from the combined GEO cohort revealed that *TRPV1* expression was significantly elevated in PTCs and PDTCs and slightly upregulated in ATCs as compared with that of the normal controls (Figure 3D). In addition, as shown in Figure 3E, in 52 paired PTC samples from the TCGA database, the mRNA expression of *TRPV1* in PTCs was greatly upregulated compared with their matched noncancerous tissues. The above results obtained from both public databases and clinical thyroid cancer samples of Jiangyuan Hospital indicated that TRPV1 was upregulated in thyroid cancers.

CAP transiently increases cytosolic Ca^{2+} concentration in ATC cells

Our recent research reported that TRPV1 was robustly expressed in PTC BCPAP cells (Xu et al., 2018). In the present study, we further detected the expression of TRPV1 channel in a nontumoral human thyroid follicular cell line (Nthy-ori-3.1) and four different ATC cell lines by reverse transcriptase PCR (RT-PCR) and western blotting. As compared to Nthy-ori-3.1 cells, the mRNA expression levels of *TRPV1* increased in ATC 8505C, FRO, and C643 cells (Figure 4A). Besides, TRPV1 protein levels were upregulated in FRO and C643 cells but in 8505C cells kept comparable to that in Nthy-ori-3.1 cells (Figure 4B). However, the basal transcriptional level of *TRPV1* kept relatively low in 8305C and C643 cells. Thus, we chose 8505C and FRO cell lines for subsequent study.

It is well-known that CAP, a potent TRPV1 agonist, can trigger a robust increase of intracellular calcium (Caterina et al., 1997). Therefore, we next detected the intracellular calcium concentration by Fluo3-AM staining using a fluorescence spectrophotometer. As shown in Figure 4C, after 200 μM CAP treatment, the fluorescence intensity of Fluo3 rose sharply in a time-dependent manner. In order to further confirm whether TRPV1, the specific receptor for CAP, was involved in CAP-induced calcium influx,
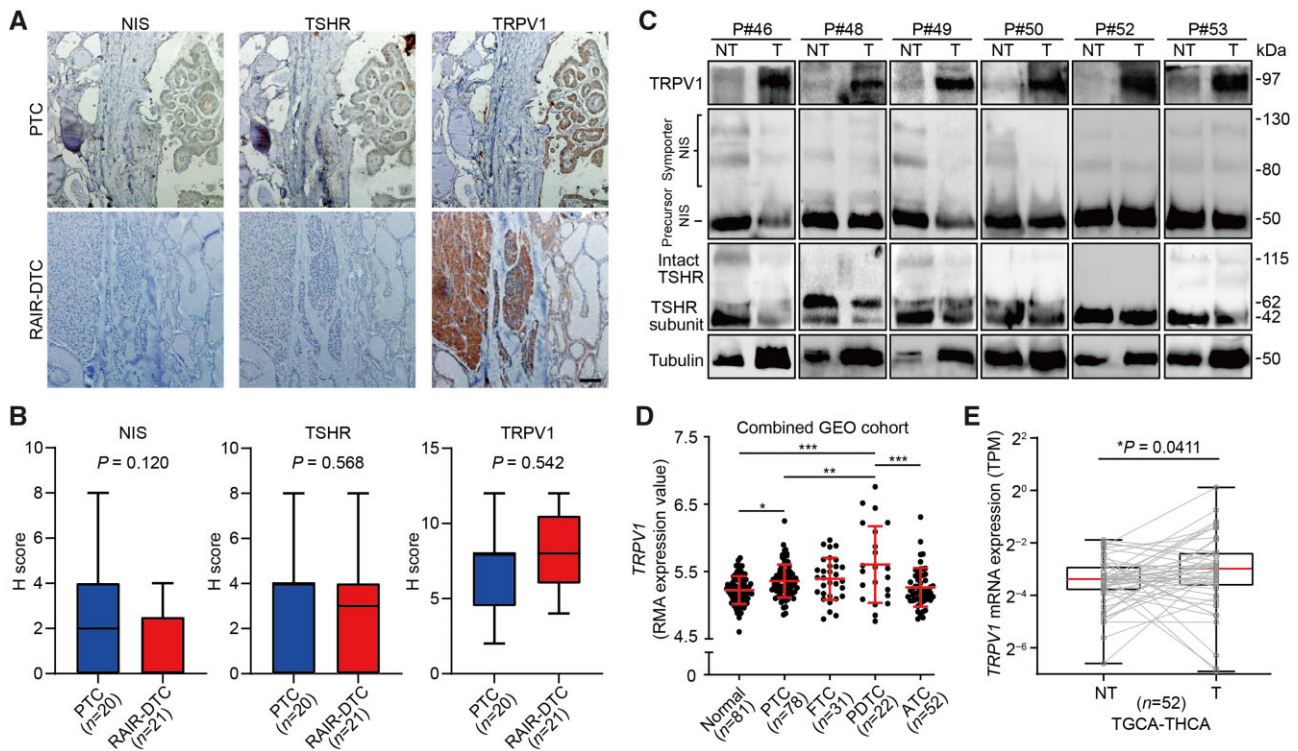
Figure 3 The expression levels of NIS, TSHR, and TRPV1 in PTC and RAIR-DTC patient samples. (**A**) IHC staining for NIS, TSHR, and TRPV1 was performed in 20 PTC and 21 RAIR-DTC samples and the representative staining images are shown. Scale bar, 100 μm. (**B**) The quantification of IHC staining against NIS, TSHR, and TRPV1 in **A**. Mann–Whitney U test. (**C**) The protein expression levels of NIS, TSHR, and TRPV1 in six PTC tumors (T) were compared with matched adjacent nontumoral thyroid tissues (NT) from the same patient. Tubulin was used as a loading control. (**D**) Bioinformatics analysis of *TRPV1* mRNA expression levels in the combined GEO cohort of thyroid cancers. *$P < 0.05$, **$P < 0.01$, ***$P < 0.001$, one-way ANOVA. (**E**) Bioinformatics analysis of *TRPV1* mRNA expression levels between PTCs and their paired adjacent normal tissues in TCGA-THCA (thyroid carcinoma) database. *$P = 0.0411$, Wilcoxon matched-pairs signed rank test.

8505C cells were pretreated with 10 μM capsazepine (CPZ), a specific TRPV1 antagonist. Expectedly, TRPV1 blockage significantly prevented calcium influx induced by CAP. Besides, the elevation of cytoplasmic calcium was completely abolished by BAPTA-AM, a calcium chelator. Consistently, as shown in Figure 4D and Supplementary Figure S3, flow cytometry results also revealed that CAP triggered a rapid accumulation of intracellular calcium in both ATC 8505C and FRO cells, which could be partially diminished by CPZ and BAPTA. In summary, these results suggested that CAP was capable of inducing a transient calcium influx through TRPV1 channel in ATC cells.

CAP activates the TRPV1–Ca^{2+}/cAMP/CREB signaling pathway in ATC cells

TSH–TSHR interaction plays a fundamental role in regulating thyroid cell proliferation, differentiation, and NIS expression through Gsα-mediated adenylyl cyclase–cAMP signaling pathway (Saito et al., 1997; Xing, 2013). The decreased expression level of TSHR was firmly confirmed in ATCs according to the results of bioinformatics analysis (Figure 1E). In addition, the reduced expression levels of cAMP and CREB were believed as the characteristics of thyroid carcinomas (Luciani et al., 2003).

Given this, targeting and activating the canonical pathway involving TSH/TSHR/cAMP to reinduce NIS expression or restore the impaired iodine-metabolizing machinery would be much ineffective in ATCs. As mentioned above, we proved that CAP could trigger a transient calcium influx through TRPV1 channel in ATC cells (Figure 4). Besides, it is well accepted that a robust Ca^{2+} influx can induce cAMP generation (Di Benedetto et al., 2013). Therefore, the elevated TRPV1 expression prompted us to propose that CAP might bypass TSHR but restore the declined NIS expression and defective radioiodine uptake of ATC cells through mediating TRPV1–Ca^{2+}/cAMP signal. As shown in Figure 5A, CAP time-dependently upregulated cAMP level in 8505C cells. Moreover, both TRPV1 antagonist (CPZ) and calcium chelator (BAPTA) exerted a strong inhibition on CAP-induced cAMP increase in 8505C (Figure 5B) and FRO cells (Supplementary Figure S4A). Hence, we concluded that CAP induced cAMP accumulation in ATC cells by triggering a TRPV1–Ca^{2+}-mediated cascade. As well-known, the increase in the concentration of either Ca^{2+} or cAMP can trigger PKA signaling. Subsequently, cAMP binds to the regulatory subunit of PKA and promotes the dissociation from the catalytic subunit. The liberated catalytic subunit will translocate into nucleus and phosphorylate CREB at Ser133, which modulates the transcription
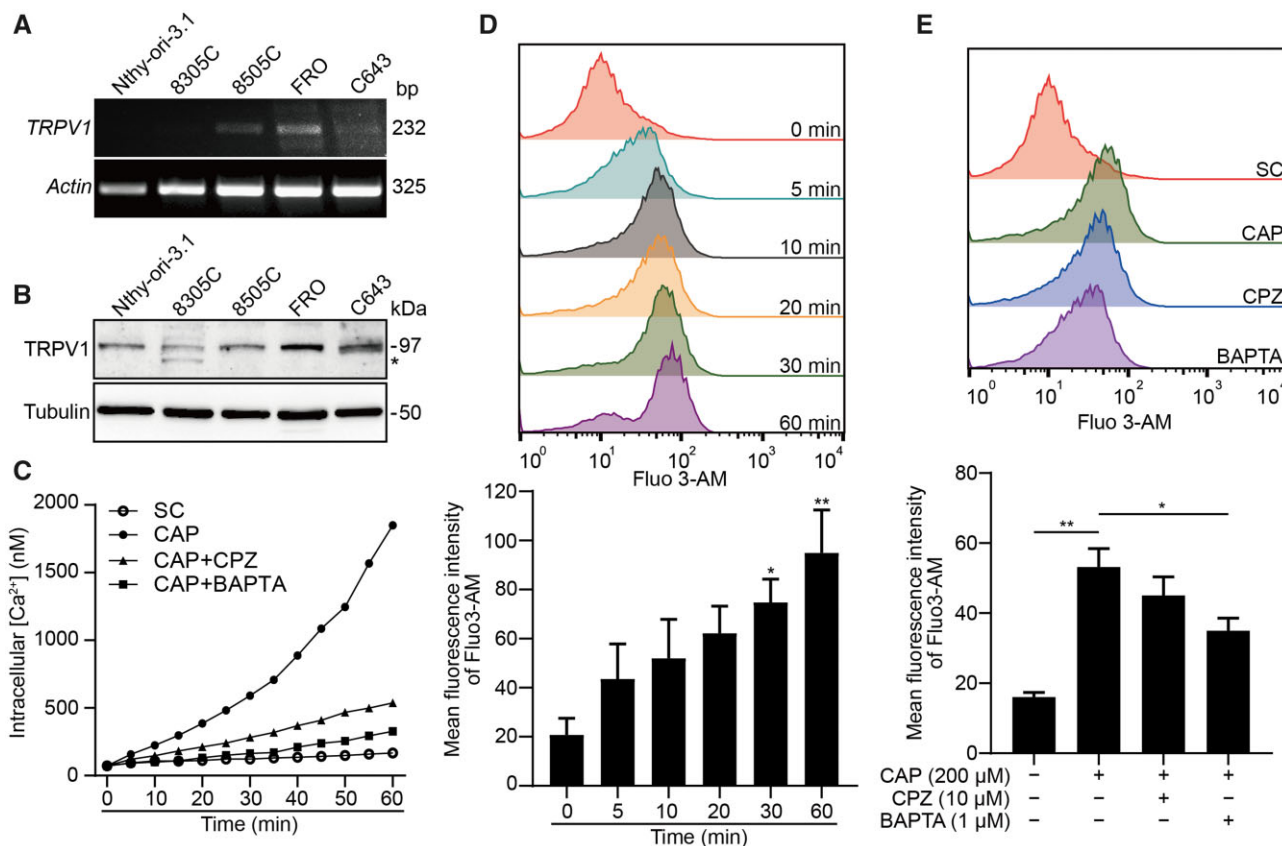
Figure 4 CAP increases TRPV1-mediated transient cytosolic Ca^{2+} influx in ATC cells. (**A**) The mRNA expression levels of *TRPV1* in a nontumoral human thyroid follicular cell line (Nthy-ori-3.1) and four ATC cell lines (8305C, 8505C, FRO, and C643) were detected by RT-PCR. (**B**) The protein expression levels of TRPV1 in Nthy-ori-3.1 and four ATC cell lines were detected by western blotting. The asterisk indicates a nonspecific band. (**C**) 8505C cells were loaded with 5 μM of Ca^{2+}-sensitive fluorescent probe Fluo3-AM and then exposed to 200 μM CAP in the presence or absence of CPZ (10 μM) or BAPTA-AM (1 μM), respectively. Calcium influx was measured by fluorescence spectrophotometer. The fluorescence signal was captured every 5 min for 1 h. (**D**) 8505C cells were loaded with 5 μM Fluo3-AM and then exposed to 200 μM CAP. Calcium influx was measured by flow cytometry every 5 min for 1 h. Quantitative analysis of the mean fluorescence intensity of Fluo3-AM was plotted against each time point. (**E**) 8505C cells were exposed to 200 μM CAP for 1 h in the presence of 10 μM CPZ or 1 μM BAPTA-AM, respectively. After cells were stained with 5 μM Fluo3-AM, the intracellular Ca^{2+} levels were analyzed by flow cytometry. Quantitative analysis of the mean fluorescence intensity of Fluo3-AM is shown at the bottom. *$P < 0.05$, **$P < 0.01$, one-way ANOVA. The data shown represent mean ± SEM of three independent experiments ($n = 3$).

of genes with cAMP-responsive elements (CREs) in their promoters (Silva et al., 1998). As expected, our results demonstrated that the phosphorylation of CREB (Ser133) was instantly increased within 5 min owing to the rapid synthesis of intracellular cAMP promoted by CAP stimulation, while the total protein level of CREB was not affected (Figure 5C). Furthermore, CPZ, BAPTA, as well as a potent and selective inhibitor of PKA, H-89, could profoundly inhibit the phosphorylation of CREB induced by CAP treatment in 8505C (Figure 5D) and FRO cells (Supplementary Figure S4B). It has been reported that certain concentration of Ca^{2+} also targeted and activated extracellular signal-regulated kinase (ERK) (Schmitt et al., 2004), which could also activate CREB (Subbiah et al., 2018). Hence, we next investigated the effect of CAP on the activation of ERK in 8505C cells. As illustrated in Figure 5C, after CAP treatment, the phosphorylation of ERK (Thr202/Tyr204) reached its peak level at

10 min and then declined steadily. Thus, CAP could activate CREB in both canonical (PKA/CREB) and noncanonical (ERK/CREB) pathways. As mentioned, upon phosphorylation, CREB becomes a functionally active form that binds to the CREs located in the promoters of target genes and activates target gene transcription. In order to further verify that CAP served as a stimulator for cAMP/PKA/CREB activation, we first constructed a CRE-reporter plasmid, pGL6-TA-4×CRE, containing quadruple CREs (TGACGTCA) located upstream of a firefly luciferase gene. As shown in Figure 5E, forskolin, a potent cAMP activator, dramatically elevated CRE-reporter luciferase activity in a dose-dependent manner with a half maximal effective concentration (EC_{50}) at 37.19 μM. Meanwhile, high concentration (>100 μM) of CAP treatment could also increase the luciferase activity and its estimated EC_{50} was 683.1 μM. Importantly, the upregulated CRE activity in CAP-treated cells was partially
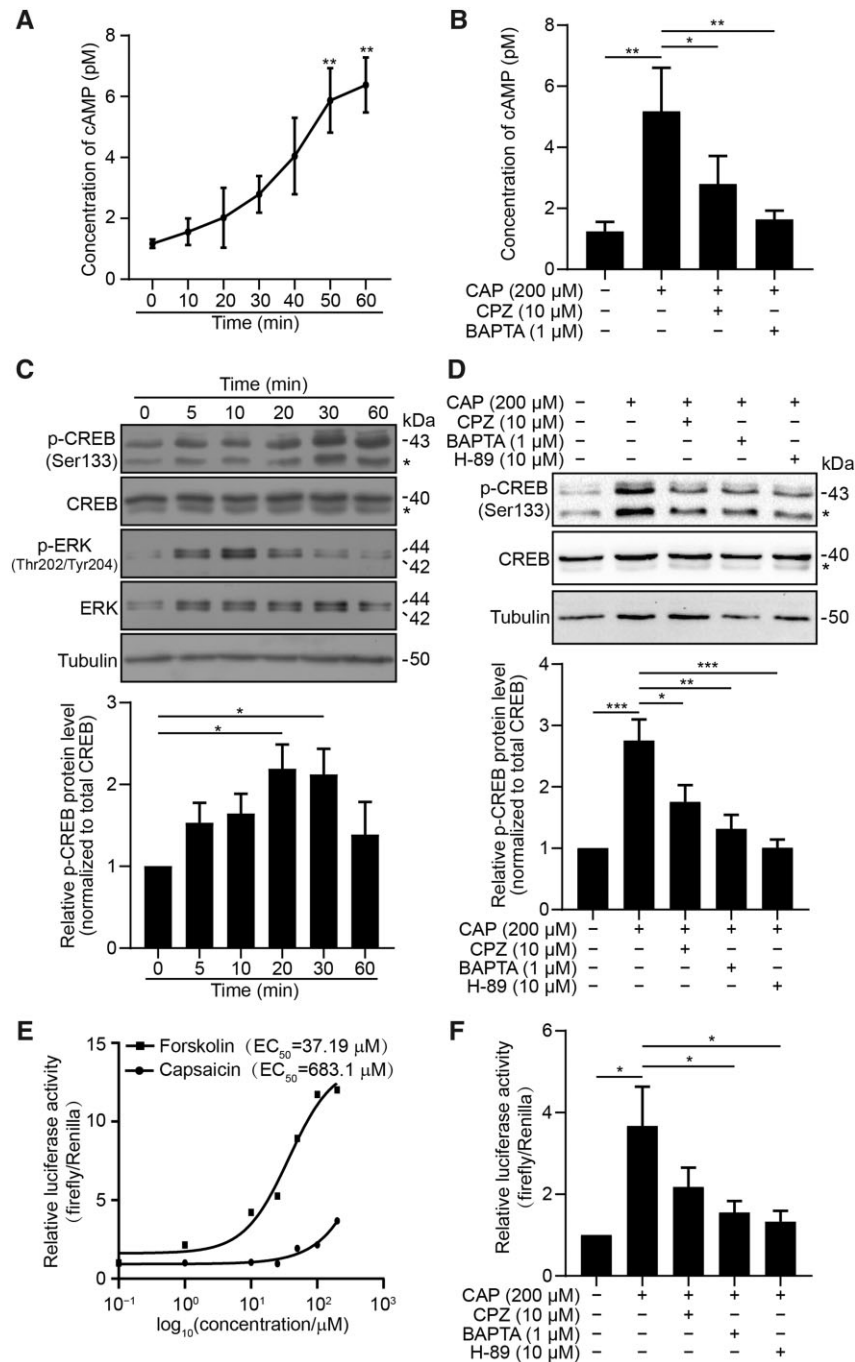
Figure 5 CAP activates cAMP/PKA/CREB signaling pathway in ATC cells. (**A**) 8505C cells were pretreated with 200 μM CAP for the indicated time periods and then the intracellular cAMP levels were measured by ELISA. The absorbance values were fit to the generated cAMP standard curve and the concentration of cAMP at each time point was calculated. (**B**) 8505C cells were exposed to 200 μM CAP for 1 h in the presence of 10 μM CPZ or 1 μM BAPTA-AM, respectively. Intracellular cAMP levels were measured by ELISA. (**C**) After 8505C cells were treated with 200 μM CAP for the indicated time periods, the protein levels of CREB, p-CREB (Ser133), ERK, and p-ERK (Thr202/Tyr204) were examined by western blotting. Tubulin was used as an internal control. The relative protein levels of p-CREB (Ser133) against total CREB at each time point was plotted at the bottom. (**D**) 8505C cells were incubated with 200 μM CAP for 1 h in the presence of 10 μM CPZ, 1 μM BAPTA-AM, or 10 μM H-89, respectively. The protein levels of CREB and p-CREB (Ser133) were analyzed by western blotting. Bottom graph shows the relative p-CREB protein level in each group normalized to total CREB. The asterisks indicate nonspecific bands. (**E**) HEK293T cells were cotransfected with 2 μg of pGL6-TA firefly luciferase reporter vector inserted with tandem 4×CREs and 0.5 μg of pRL-TK. After transfection for 24 h, the cells were treated with different dosages of CAP or forskolin for another 6 h. Dual-luciferase reporter system was used to evaluate the signal of the constructed luciferase reporter. Renilla luciferase was used as an internal control. Dose–response curve was generated and the drug EC_{50} was further calculated. (**F**) HEK293T cells were transfected as in **E**, and then the cells were further treated with 200 μM CAP for 6 h in the presence of 10 μM CPZ, 1 μM BAPTA-AM, or 10 μM H-89, respectively. Luciferase reporter assay was performed. *$P < 0.05$, **$P < 0.01$, ***$P < 0.001$, one-way ANOVA. The data shown represent mean ± SEM of three independent experiments ($n = 3$).

alleviated by CPZ, BAPTA, or H-89 addition (Figure 5F), indicating that TRPV1−Ca^{2+}/cAMP/PKA pathway was involved in CAP-induced CREB activation.

CAP triggers the transcription of SLC5A5 through CREB activation

Our luciferase reporter assay proved that CAP treatment sharply increased the phosphorylation of CREB and the transcriptional activity of downstream CRE. Hence, we ought to examine whether CREB could promote *SLC5A5* transcription in ATC cells. As shown in Figure 6C, the putative binding sites of canonical CREB (TGACGTCA) at the promoter of *SLC5A5* (−2000 to +200 nt) was predicted by JSPAR (http://jaspar.gen ereg.net/). There were a total of 11 predicted binding sites of CREB on the promoter of *SLC5A5* (−2000 to +200 nt) (detailed in Supplementary Table S3). Owing to the high GC content and complex DNA structure of *SLC5A5* promoter, we only got the −1057 to +200 nt fragment of *SLC5A5* promoter, which contained 7 out of 11 predicted CREB binding sites, but failed to obtain its longer fragment (−2000 to +200 nt) after a variety of attempts. We tried to perform dual-luciferase reporter assay in ATC cells but the transfection efficiency of all the ATC cell lines we tested (850C and FRO) was relatively low. Alternatively, we chose the PTC cell line BCPAP, which has a higher transfection efficiency. As shown in Figure 6A, bCPAP cells transfected with the full-length *SLC5A5* promoter (−1057 to +200 nt) exhibited an ~2.3-fold induction in luciferase activity by CAP treatment. Noticeably, the TRPV1 antagonist CPZ, the calcium chelator BAPTA, and the PKA inhibitor H-89 effectively abolished the CAP-upregulated transcriptional activity of the *SLC5A5* promoter. In order to further identify the specific binding motifs of CREB on *SLC5A5* promoter, three luciferase reporters with different lengths of *SLC5A5* promoter were constructed. The shorter truncated promoter (−512 to +200 nt) showed a declined luciferase activity in comparison with the full-length *SLC5A5* promoter. Besides, the luciferase activity decreased to a background level as the reporter harbored the region from −136 to +200 nt, suggesting that CREB lost its binding to an upstream region of the *SLC5A5* promoter lacking the region from −1057 to −512 nt. These results indicated that CREB mainly recognized and bound to the region from −1057 to −512 nt of *SLC5A5* promoter and activated its transcription (Figure 6B). Furthermore, the functionality of putative CREs responsible for CREB recognition within this promoter region was evaluated. Hence, an indicated region of *SLC5A5* promoter (−1057 to −695 nt) carrying the three wild-type functional CRE sequences or the same sequences with substitutions A to C (A>C) and G to T (G>T) in highly conserved nucleotide sequences of each CRE were cloned. The fragments containing the wild-type or the mutated CREs were, respectively, inserted into pGL6-TA (Figure 6C and D). Notably, changes of highly conserved A>C and G>T in the first two putative CRE sequences (M1 and M2 mutations) and a

substitution A>C in the third CRE (M3 mutation) all impaired *SLC5A5* promoter activity (Figure 6E). Above all, these findings showed that CAP treatment facilitated CREB to bind to and activate at least three CREs in the region from −1057 to −512 nt of *SLC5A5* promoter through TRPV1−Ca^{2+}/cAMP/PKA cascade.

CAP partially restores NIS-mediated radioiodine uptake of ATC cells

In the present study, we confirmed that CAP could target CREB and upregulate NIS gene expression by activation of the TRPV1−Ca^{2+}/cAMP/CREB signaling pathway. These striking results promoted us to explore whether CAP could restore ^{131}I uptake of ATC cells. As expected, CAP increased the mRNA level of *NIS* and protein level of mature glycosylated NIS in ATC cells (Figure 7A; Supplementary Figure S5A). Subsequently, an *in vitro* [131]I uptake assay was performed. As shown in Figure 7B; Supplementary Figure S5B, the uptake of ^{131}I by ATC cells was significantly increased after CAP treatment. Meanwhile, TRPV1 antagonist (CPZ), calcium chelator (BAPTA), and PKA inhibitor (H-89) effectively suppressed the elevated NIS mRNA and protein levels (Figure 7A and B) and ^{131}I uptake (Figure 7C) induced by CAP in both 8505C and FRO cells. Furthermore, we observed an inhibitory effect of CAP combined with radioiodine on the colony formation of 8505C cells. As shown in Figure 7C, when treated with radioiodine (0.925 MBq) or CAP (200 μM) alone, the colony formation of 8505C cells was inhibited to a certain extent. Strikingly, when the cells were pretreated with CAP followed by radioiodine, almost no tumor clone was formed. These results suggested that CAP enhanced the uptake of ^{131}I and sensitized ATC cells to radioiodine treatment.

Discussion

It is well-known that radioiodine therapy is a highly effective oncologic therapy in DTC. TSH-mediated activation of TSHR is proved to be able to augment radioiodine therapeutic efficiency (Xing, 2013). Hence, in clinical practice, rTSH supplement is routinely used to achieve adequate TSH levels prior to radioiodine therapy (Fast et al., 2011). However, ATC is a subtype of undifferentiated thyroid carcinoma, which is extremely aggressive and characterized by the impairment of the iodine-metabolizing machinery owing to the aberrant silence of thyroid functional genes (Xing, 2013). Consistent with these notions, we found that thyroid differentiation markers, including *TTF-1*, *TTF2*, *PAX8*, *TPO*, *NIS*, and *TSHR*, were aberrantly absent in PDTC/ATC samples of a combined GEO cohort of thyroid cancers (Figure 1). As a consequence, virtually all cases of ATC are refractory to conventional radioiodine therapy and handling ATC is a major clinical challenge (Maniakas et al., 2020). Moreover, we also observed silenced expression of NIS and TSHR in some RAIR-DTCs and PTCs collected by Jiangyuan Hospital (Figure 3).
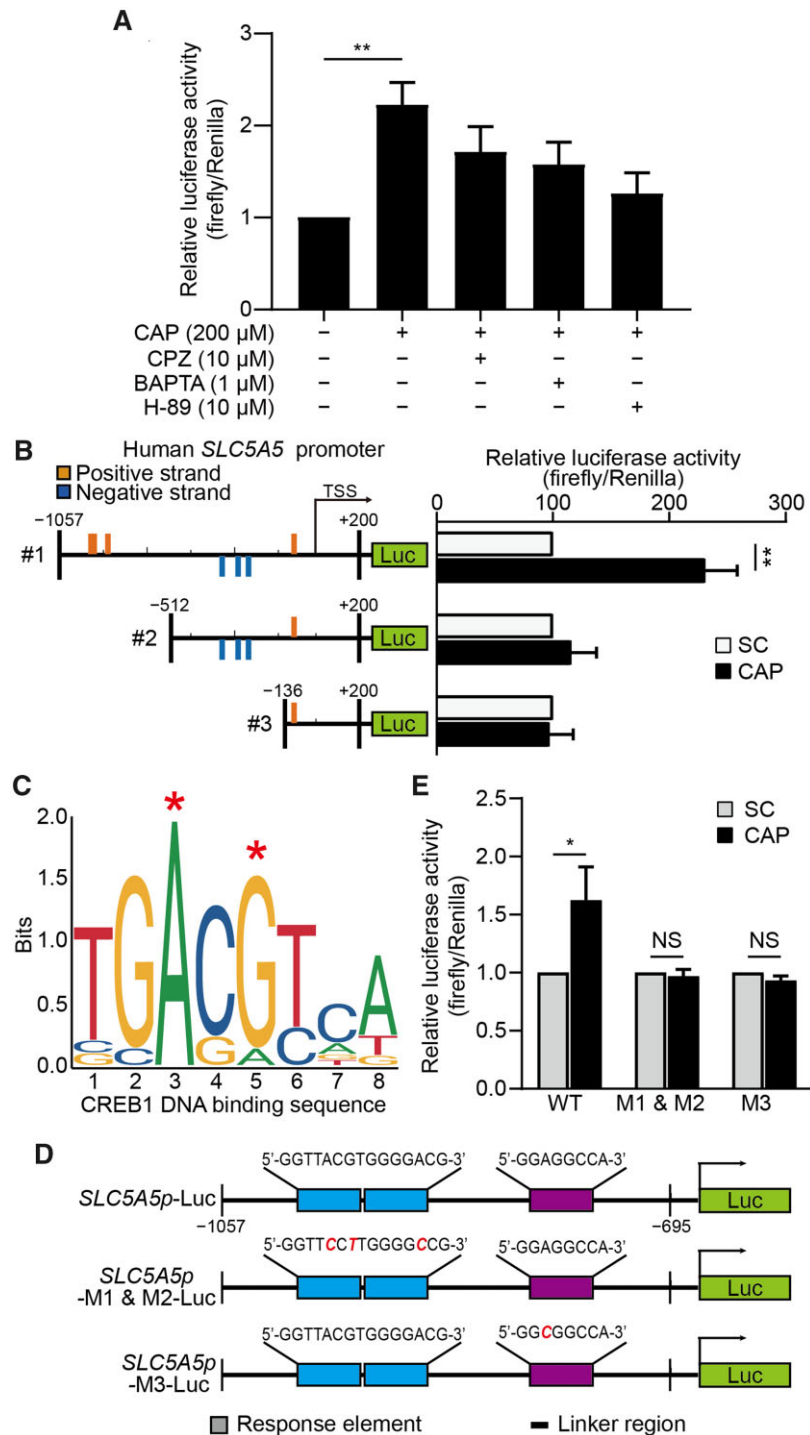
Figure 6 CAP triggers the transcription of *SLC5A5* through CREB activation. (**A**) BCPAP cells were transfected with the full-length *SLC5A5* promoter (#1: −1057 to +200 nt) plasmid and then treated with 200 μM CAP for 24 h in the presence of 10 μM CPZ, 1 μM BAPTA-AM, or 10 μM H-89, respectively. Luciferase activity was measured by the dual-luciferase assay, and Renilla luciferase was used as an internal control. *******P* < 0.01, one-way ANOVA. (**B**) The 5′ stepwise truncations of *SLC5A5* promoter (#1: −1057 to +200 nt; #2: −512 to +200 nt; #3: −136 to +200 nt) were cloned into pGL6-TA plasmid. BCPAP cells were individually transfected with the truncated *SLC5A5* promoter plasmids and then treated with or without 200 μM CAP for 24 h. Luciferase reporter assay was performed. *******P* < 0.01 vs. SC, Student's *t*-test. (**C**) The DNA binding sequence of CREB was predicted by JASPAR (http://jaspar.genereg.net/). The bigger a letter is, the more conserved is the nucleotide in that position among different already known CREs. The asterisks show the nucleotide substitutions. (**D**) Luciferase reporter constructs carrying the three wild-type predicted functional CRE sequences and the same sequences with substitutions A>C and G>T of indicated nucleotide sites from *SLC5A5* promoter (located in the region from −1057 to −695 nt) were cloned into pGL6-TA plasmid. (**E**) BCPAP cells were transfected with 2 μg wild-type (WT) and mutated reporters, respectively, and then treated with 200 μM CAP for 24 h. Luciferase activity was measured, normalized to Renilla activity, and presented as fold of change. **P* < 0.05, one-way ANOVA. NS, no significance. The data shown represent mean ± SEM of three independent experiments (*n* = 3).

Accumulating studies have highlighted the fact that TSH–TSHR serves as a major regulator of NIS expression (Vassart and Dumont, 1992) and NIS post-translational modification, which is essential for its trafficking to the membrane (Riedel et al., 2001). TSHR is a guanine-nucleotide binding G-protein-coupled receptor. When activated by TSH, it triggers downstream Gsα-mediated adenylyl cyclase–cAMP signaling and further modulates the expression and activity of NIS, resulting in iodine uptake (Ben Abdelkhalek et al., 1994). It has also been reported that cAMP is a cellular second messenger that converts the extracellular stimuli into specific targets through activating PKA and CREB, which influences a wide range of cellular processes including gene transcription, cell proliferation, migration, and mitochondrial homeostasis (Gancedo, 2013). A latest research indicated that an antiretroviral compound, nevirapine, could increase NIS expression and radioiodine uptake through activating the TSHR/cAMP/CREB/PAX8 signaling pathway in dedifferentiated thyroid cancer (Shang et al., 2020). Unfortunately, as mentioned above, TSHR was proved abnormally decreased in ATC, making the impairment of TSH–TSHR machinery to regulate NIS (Landa et al., 2016). Thus, seeking new ways to reinduce NIS expression and restore radioiodine uptake is worthy of further research in PDTC/ATC therapy.

There is a cross-talk between calcium and cAMP signaling. For example, it has been reported that calcium influx could stimulate the production of cAMP and induce the activation of PKA in the central nervous (Cameron and Kapiloff, 2017). Besides, calcium was also discovered to potentiate cAMP generation and insulin secretion in insulinoma MIN6 cells (Kitaguchi et al., 2013). These results enlightened us to investigate the potential of modulating calcium signal to upregulate cAMP concentration through bypassing TSH–TSHR machinery. Our recent study proved that CAP triggered calcium overload through TRPV1 and induced apoptosis in ATC cells (Xu et al., 2020a). In the present study, we demonstrated that CAP induced calcium influx (Figure 4) and elevated intracellular cAMP concentration through TRPV1 in ATC cells (Figure 5). Strikingly, we found that CAP could restore the expression of iodine-metabolizing genes in human ATC cells to a certain degree (Figure 2). It is worth noting that CAP could not only increase the expression of NIS but also enhance the membrane localization of NIS protein, leading to a remarkably enhancement of radioiodine uptake in ATC cells (Figures 2 and 7). Martin et al. (2019) reported that adaptor protein-1B (AP-1B) recognized the monoleucine-based sorting motif in NIS carboxy-terminus and regulated NIS plasma membrane transport. Furthermore, the detailed mechanism involved in the plasma membrane trafficking induced by CAP is worthy of further research as a comprehensive topic.

CAP is a well-known TRPV1 agonist. TRPV1 is a nonselective cation channel, which can be potently activated by high temperature, low pH, and multiple chemical stimuli, especially CAP (Caterina et al., 1997). Interestingly, distinct from the loss of iodine-metabolizing genes, our bioinformatics analysis of the combined GEO cohort and the TCGA dataset of thyroid cancers demonstrated that TRPV1 expression was significantly increased in thyroid tumors compare to the adjacent nontumoral

thyroid tissues (Figure 3). In line with these findings, IHC staining results obtained from our own PTC/RAIR-DTC cohort also confirmed that TRPV1 expression elevated in RAIR-DTC to some extent (Figure 3). Thus, the positive expression of TRPV1 provided a premise possibility for triggering TRPV1-mediated calcium influx and subsequent cAMP accumulation in ATC cells.

As known, an increase in cAMP triggers PKA signaling. cAMP binds to the regulatory subunit of PKA and dissociates it from the catalytic subunit. The liberated catalytic subunit enters the nuclear and phosphorylates CREB at Ser133. Then, the activated CREB promotes the transcription of target genes, which harbor CRE motifs on their promoters (Altarejos and Montminy, 2011). Consistently, our study revealed that CAP treatment could promote CREB phosphorylation and augment its transcriptional activity through activating calcium/cAMP/PKA cascade (Figure 5). In order to further explain the potential mechanism by which CAP reinduced the expression of iodine-metabolizing genes, we searched CREs at the promoter of *SLC5A5* gene, which encodes NIS. It should be noted that our study first discovered the presence of a cluster of positive regulatory CREs in the region from −1057 to −512 nt of *SLC5A5* promoter, which was responsible for CREB binding (Figure 6).

Surprisingly, our study highlighted the fact that CAP treatment induced a significant improvement of radioiodine avidity in ATC cells (Figure 7). However, the specific mechanisms behind the upregulation of other iodine-metabolizing genes (such as *TTF-1*, *PAX8*, *TSHR*, and *TPO*) by CAP treatment remained unclear. It has been reported that the increase in intracellular calcium directly upregulated TTF-1 expression in thyroid parafollicular C cells (Suzuki et al., 1998). Besides, the activation of cAMP stimulated by rTSH could coordinately induce the transcription of *NIS*, *TPO*, and *TG* (Paz-Filho and Graf, 2008). Therefore, it is reasonable for us to speculate that CAP may increase the expression of these iodine-metabolizing genes through promoting calcium influx as well. Further studies to clarify the mechanisms involved are clearly warranted. It is also worth noting that CAP exerted potent anticancer effects against certain types of cancer in both Ca^{2+}-dependent and Ca^{2+}-independent mechanisms (Clark and Lee, 2016). For example, CAP could directly target the EGFR-mediated FAK/AKT, PKC/Raf/ERK, p38/MAPK, and AP-1 signaling pathways to suppress human fibrosarcoma cell metastasis (Hwang et al., 2011). In the present study, although we could not rule out the potential possibility that certain Ca^{2+}-independent mechanisms may participate in the redifferentiating efficacy of CAP on ATC cells, our results provide persuasive evidence that the redifferentiation of ATC cells induced by CAP was primarily dependent on the increase in intracellular calcium through TRPV1 channel activation.

In conclusion, this study demonstrated that CAP could directly trigger calcium influx through modulating TRPV1 channel, leading cAMP signal activation in ATC cells. Notably, CAP partially restored NIS expression and function mainly through triggering CREB to bind to the promoter of *SLC5A5*, which
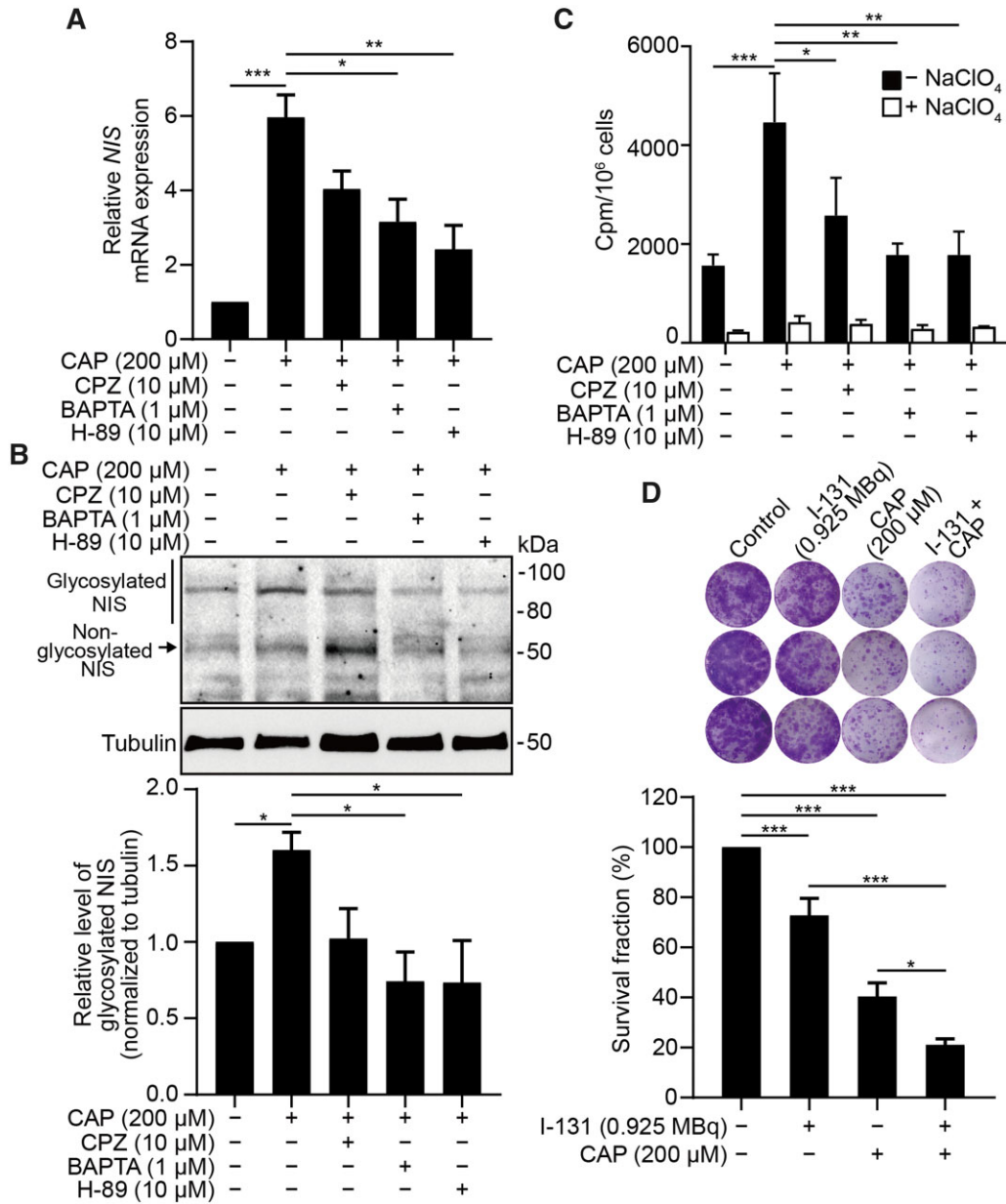
Figure 7 CAP restores NIS-mediated radioiodine uptake of ATC cells. (**A** and **B**) 8505C cells were treated with 200 μM CAP for 24 h in the presence of 10 μM CPZ, 1 μM BAPTA-AM, or 10 μM H-89, respectively, and then the mRNA expression level of *NIS* was examined by qPCR (**A**) and NIS protein level was analyzed by western blotting (**B**). Representative western blots are shown on the top. Bottom graph shows the quantification of glycosylated NIS levels normalized to Tubulin. (**C**) 8505C cells were treated with 200 μM CAP for 24 h in the presence of 10 μM CPZ, 1 μM BAPTA-AM, or 10 μM H-89, respectively. Then, the cells were further incubated with 37 kBq $Na^{131}I$ for 1 h in the presence or absence of 100 μM $NaClO_4$. After rounds of wash, the radioiodine accumulated in 8505C cells was measured using a gamma-counter. (**D**) 8505C cells were pretreated with CAP in the presence of 10 μM CPZ, 1 μM BAPTA-AM, or 10 μM H-89, respectively, for 6 h. Then, cells were counted and seeded into 24-well plates and incubated with 0.925 MBq $Na^{131}I$ for another 24 h. After 10 days, surviving colonies were stained with crystal violet and images were captured. The cell survival fraction was calculated. *$P < 0.05$, **$P < 0.01$, ***$P < 0.001$, one-way ANOVA. The data shown represent mean ± SEM of three independent experiments ($n = 3$).

encodes NIS. Subsequently, CAP dramatically increased the iodine uptake and radiosensitivity of ATC cells *in vitro*. These findings suggest that CAP can stimulate the redifferentiation of TSHR-impaired ATC cells to a certain extent. Of note, CAP may afford a novel therapeutic strategy to treat ATC, which is refractory to radioiodine treatment.

Materials and methods

Chemicals, reagents, and antibodies

Capsaicin (CAP) and H-89 were purchased from Sigma-Aldrich. Capsazepine (CPZ) was purchased from MedChem Express. BAPTA-AM was purchased from Adooq Bioscience. Methyl thiazolyl tetrazolium (MTT) was purchased from Sangon. Fluo3-AM was obtained from Yeasen Biotechnology. Forskolin was purchased from Beyotime Institute of Biotechnology. Recombinant human TSH alpha/beta heterodimer (4610-TH-10) was purchased from R&D systems. Sodium iodine (^{131}I) oral solution (Chengdu Nuclear High-Tech Co., Ltd.) was provided by the Department of Nuclear Medicine of the Affiliated Hospital of Jiangsu Institute of Nuclear Medicine. Primary antibodies used in the present study were as follows: anti-NIS (sc-134515), anti-TSHR (sc-13936), anti-TTF-1 (sc-53136), and anti-GAPDH (sc-32279) antibodies were purchased from Santa Cruz Biotechnology; anti-Pax8 (CST#59019), anti-ERK (CST#4695), and anti-phospho-ERK (Thr202/Tyr204, CST4370) antibodies were purchased from Cell Signaling Technology; anti-CREB (AF6566), anti-phospho-CREB (Ser133, AF5785), and anti-β-tubulin (AT819) antibodies were purchased from Beyotime Institute of Biotechnology; anti-TRPV1 (bs-1931R) and anti-TPO (bs-0447R) antibodies were purchased from Bioss. Secondary antibodies, goat anti-rabbit (A0208) and goat anti-mouse (A0216) IgG-HRP, were purchased from Beyotime Institute of Biotechnology. Other chemicals were analytical grade and purchased from common commercial source.

Cell culture and drug treatments

The nontumoral human thyroid follicular cell line Nthy-ori-3.1 and anaplastic thyroid cancer (ATC) cell line 8505C were purchased from the European Collection of Cell Cultures (ECACC) (passage number <10). PTC cell line BCPAP and ATC cell lines 8305C, FRO, and C643 (passage number <5) were obtained from Shanghai Institute of Biochemistry and Cell Biology (Shanghai, China). Nthy-ori-3.1, FRO, and C643 cells were maintained in RPMI 1640 media containing 10% fetal bovine serum (FBS). 8505C cells were maintained in MEM containing 10% new-born calf serum (NBS). BCPAP cells were maintained in RPMI 1640 media containing 10% FBS, 1% sodium pyruvate, 1% glutamine, and 1% nonessential amino acids. 8305C cells were maintained in MEM containing 10% FBS, 1% glutamine, and 1% nonessential amino acids. The cell culture media was supplemented with 100 U/ml penicillin and 100 U/ml streptomycin. These cell lines were incubated under a humid atmosphere of 5% (v/v) CO_2 at 37°C. CAP was dissolved in dimethyl sulfoxide (DMSO) to a stock concentration of 200 mM and stored at −20°C. Capsazepine was dissolved in DMSO to a concentration of 20 mM and stored at 4°C. BAPTA-AM and H-89 were dissolved in DMSO to a stock concentration of 10 mM and stored at −20°C. These stock solutions were diluted before use. Unless otherwise indicated, solvent control contains equal amount of solvent to that of the highest concentration of the corresponding drug. To be pointed out, the final solvent concentration did not exceed 0.1% (v/v) in any experiment.

Bioinformatics analysis

Raw microarray files in CEL format of GSE29265, GSE35570 (Handkiewicz-Junak et al., 2016), GSE76039 (Landa et al., 2016), GSE65144 (von Roemeling et al., 2015), GSE82208 (Wojtas et al., 2017), and GSE53157 (Pita et al., 2009) profile datasets were downloaded from the GEO database (http://www.ncbi.nlm.nih.gov/geo/). These datasets were performed on the same chip platform GPL570, which is Human Genome U133 Plus 2.0 Array platform (Affymetrix; Thermo Fisher Scientific, Inc.). These six datasets contained 81 nontumoral/normal thyroid tissues, 76 PTC tissues, 31 FTC tissues, 22 PDTC tissues, and 52 ATC tissues. These files were background adjusted and normalized using robust multichip average (RMA) methodology (Bolstad et al., 2003) and RMA Express program was available at the website http://rmaexpress.bmbolstad.com. The ComBat method was used to remove the batch effects. When multiple probes corresponded to the same gene, the average value was used as the expression level of this gene. All probes were mapped to the latest version of the Affymetrix NetAffx annotation file.

Tumor sample collection

A total of 41 paraffin-embedded tissues of thyroid cancer patients who underwent thyroid surgery from January 2013 to December 2019 were collected by Jiangyuan Hospital, which is the affiliated hospital of Jiangsu Institute of Nuclear Medicine. Besides, 12 pairs of fresh PTC tissues were obtained from the patients who underwent thyroid surgery. Our cohort contained 21 RAIR-DTCs. Patients were enrolled as RAIR-DTC if they met one of the following criteria: (i) who had at least one measurable lesion without iodine uptake on ^{131}I scan; (ii) who had one measurable lesion that had progressed within the past 12 months even it could take up radioiodine; and (iii) who received cumulative activity of ^{131}I over 600 mCi (22.2 GBq) (Gao et al., 2019). For IHC staining, samples were fixed with formalin and then embedded using paraffin. For western blotting analysis, samples were immediately snap-frozen in liquid nitrogen and stored at −80°C. All clinical samples were collected with the approval of the ethics committee of Jiangsu Institute of Nuclear Medicine.

Immunohistochemistry

Tumor samples were fixed in 10% buffered formalin for 24 h followed by embedding in paraffin, and sliced into 4-μm-thick sections using manual rotary microtome (Leica HistoCore BIOCUT). For antigen retrieval, the slides were rehydrated and then incubated with 10 mM of heated sodium citrate buffer (pH 6.0) for 20 min. Subsequently, the slices were treated with 3% H_2O_2 for 15 min to block endogenous peroxidase activity and then blocked with 1% bovine serum albumin for 1 h at room temperature (RT). Then, the slices were incubated with the indicated primary antibodies at 4°C overnight, followed by incubation with HRP-conjugated secondary antibody

for 1 h at RT. Immunoreactive signal was visualized with a DAB Substrate Kit (MXB Biotechnologies). The expression levels of the target proteins in all the samples were scored according to the percentage of immunopositive cells and immunostaining intensity. The following antibodies were used for IHC: NIS (1:100, Santa Cruz, sc-134515), TSHR (1:100, Santa Cruz, sc-13936), and TRPV1 (1:100, Bioss, bs-1931R). Staining results were assessed independently by two pathologists without prior consultation using a scoring system modified by Lu et al. (1998), where the staining intensity in the malignant cell was scored as 0, 1, 2, or 3 corresponding to the presence of negative, weak, moderated, and strong staining, respectively. Besides, the total number of cells in each field and the number of cells stained at each intensity were counted, and the mean percentage of positive-stained cells was assigned to one of the following categories: $0 \leq 5\%$; $1 = 5\%–25\%$; $2 = 25\%–50\%$; $3 = 50\%–75\%$; and $4 \geq 75\%$. The percentage of positive-stained cells and the staining intensity were ultimately multiplied to produce a weighted score for each case.

Western blotting

Cell lysis and western blotting were performed as previously reported (Xu et al., 2018). Briefly, the whole-cell lysates were extracted by RIPA buffer (Beyotime) supplemented with protease inhibitor cocktail (Sangon Biotech). Membranal and cytoplasmic proteins were extracted using the Membrane and Cytosol Protein Extraction Kit (Beyotime) according to the manufacturer's instruction. Equal amounts of proteins were initially denatured at 95°C for 5 min, separated by 8%–12% sodium dodecyl sulfate-polyacrylamide gel electrophoresis and transferred to a nitrocellulose membrane (Millipore). Then, the membranes were blocked with 5% skimmed milk and probed with indicated primary antibodies at 4°C overnight. Subsequently, the membranes were incubated with indicated HRP-conjugated anti-rabbit or anti-mouse secondary antibody for another 1 h at RT. After that, the membranes were visualized using an enhanced chemiluminescence (ECL) western blot kit (Absin Bioscience). Images were captured by a protein gel imaging system (ChemiDoc XRS+, Bio-Rad). The protein bands were analyzed and quantified using ImageJ software.

RT-PCR and qPCR

Total RNA was extracted using TRIzol reagent (CWBIO) according to the manufacturer's instructions. First-strand cDNA was synthesized from 2 μg of total RNA using MLV-reverse transcriptase (TaKaRa) and oligo $(dT)_{18}$ primers. RT-PCR was performed using the following procedure: initial denaturation at 95°C for 5 min, and then 30 cycles of amplification with denaturation at 95°C for 30 sec, annealing at 60°C for 30 sec, and elongation at 72°C for 30 sec, and a final extension at 72°C for 5 min. The primer sequences for RT-PCR are listed in Supplementary Table S4. PCR products were electrophoresed

in 2% agarose gel and visualized by ethidium bromide dying. qPCR was performed in an ABI 7500 Real-time PCR detection system (Applied Biosystems). SYBR Green mixture (CWBIO) was used as PCR buffer and the amplification parameters were as follows: initial denaturation at 95°C for 5 min, 40 cycles of denaturation at 95°C for 15 sec, and annealing at 60°C for 60 sec. For each sample, the mRNA levels of target genes were normalized against the house-keeping gene *GAPDH* using $2^{-\Delta\Delta Ct}$ (Livak) method. The target gene/*GAPDH* ratios were then normalized against those in control samples. The primer sequences for qPCR are listed in Supplementary Table S4.

In vitro ^{131}I uptake assay

Cellular ^{131}I uptake assay was performed as previously described with some modifications (Weiss et al., 1984). Briefly, 8505C and FRO cells (1×10^5 cells/well) were seeded into 12-well plates and incubated with CAP for 24 h at 37°C. After incubation, the medium was aspirated and the cells were washed with Hank's balanced salt solution (HBSS). Then, cells were incubated with 500 μl HBSS containing 37 kBq carrier-free $Na^{131}I$ and 10 μM sodium iodine at 37°C for 1 h. After incubation, cells were washed with ice-cold PBS for three times and lysed with 500 μl of 0.1 M NaOH and then the radioactivity was read by a gamma-counter (2470, PerkinElmer). The count per minute (Cpm) was measured and the values were normalized with the counted cell numbers of the parallel wells. The cellular ^{131}I uptake was expressed as $Cpm/10^6$ cells. Besides, the cells were preincubated for 15 min with 100 μM $NaClO_4$, a competitive inhibitor of NIS (Josefsson et al., 2006), before adding $Na^{131}I$.

Measurement of intracellular calcium

The cytoplasmic calcium was measured by a flow cytometer (Becton Dickinson FACS Calibur) or a fluorescence spectrophotometer (PerkinElmer LS 55) as previously described with some modifications (Wang and Xu, 2005). For flow cytometry analysis, cells were harvested and loaded with 5 μM Fluo3-AM for 30 min in the dark. After staining, 200 μM CAP in the absence or presence of 10 μM CPZ or 1 μM BAPTA-AM was added into the cell suspension, and then the Fluo3-AM signals were detected by flow cytometry at indicated time points at FL1 channel. For kinetic intracellular Ca^{2+} level detection, cells (5×10^5) were stained with 5 μM Fluo-3AM and resuspended in 200 μl Krebs–Ringer–HEPES buffer (131 mM NaCl, 5 mM KCl, 1.3 mM $MgSO_4$, 1.3 mM $CaCl_2$, 0.4 mM KH_2PO_4, 6 mM glucose, 20 mM HEPES, pH 7.4). Then, the cells were treated with 200 μM CAP in the absence or presence of 10 μM CPZ or 1 μM BAPTA-AM. The fluorescence (F) was determined using a fluorescence spectrophotometer with excitation and emission wavelengths at 488 and 526 nm, respectively, every 5 min. Intracellular Ca^{2+} was calculated using the following equation: $[Ca^{2+}]i = K_d[(F - F_{min})/(F_{max} - F)]$, where K_d of Fluo-3 is 400 nM

(Merritt et al., 1990). The maximal Fluo-3 fluorescence intensity (F_{max}) was determined by adding 0.1% Triton X-100, while the minimal fluorescence (F_{min}) was determined by quenching Fluo-3 fluorescence with the addition of 5 mM EGTA.

cAMP concentration measurement

Intracellular cAMP was measured by a cAMP-specific ELISA kit (Bioyears, Wuhan) according to the manufacturer's protocol. Briefly, all reagents were brought to RT before use. First, cells were lysed by 0.1 M HCl. After that, 100 µl of extracted sample or standard and 100 µl of conjugated antibody were simultaneously added into a 96-well microplate, which was precoated with the capture antibody against human cAMP. Then, the plate was covered with the adhesive strip. After incubation for 2 h at RT, the supernatant was aspirated, and each well was washed for three times using washing buffer. After the last wash, the remaining buffer was removed by aspiration or decantation. Subsequently, 50 µl of substrate solution was added to each well. After incubation for another 15 min at RT, 50 µl of stop solution was added into each well, and the optical density of each well was measured immediately using a microplate reader at 450 nm. A standard curve was constructed by plotting the absorbance for each standard sample on the y axis against the cAMP concentration on the x axis and fitted by regression analysis. Then, the concentration of cAMP in each sample was calculated according to the generated standard curve.

Plasmid construction

Quadruple CREs (TGACGTCA) were synthesized at Sangon Biotech (Shanghai) and cloned into pGL6-TA luciferase vector (Beyotime) and the constructed plasmid was named as pGL6-TA-4×CRE. Besides, a series of truncated human *SLC5A5* promoters were subcloned into *Kpn*I/*Hin*dIII cloning site of pGL6-TA luciferase vector. Three regions of *SLC5A5* promoter (#1: −1057 to +200 nt; #2: −512 to +200 nt; #3: −136 to +200 nt) were amplified from pGL2-Basic-NIS promoter plasmid, which was kindly provided by Prof. Xiaotao Li (Jiao et al., 2020), using forward primers 5′-*GGTACC*TCCACC CTGCACAGCAGAGA-3′ (#1), 5′-*GGTACC*GCGTGATTGCCCAGAA AGTT-3′ (#2), and 5′-*GGTACC*GAATGAGGCACTTATCATGT-3′ (#3), respectively, and the same reverse primer 5′-*AAGCTT* GGGAGCTCACTTTCATGCA-3′. For mutations in putative CRE sequences, oligonucleotides containing the region from −1057 to −695 nt of *SLC5A5* promoter with three functional CREs were subcloned into pGL6-TA luciferase vector; meanwhile, the same sequences with substitutions G>T and A>C were constructed. All the constructs were then verified by Sanger sequencing at Sangon Biotech.

Luciferase reporter assay

BCPAP cells were cotransfected with 2 µg of pGL6-TA firefly luciferase reporter vector (Beyotime) inserted with different regions of *SLC5A5* promoter (region #1: −1057 to +200 nt; region #2: −512 to +200 nt; region #3: −136 to +200 nt) and 0.5 µg of pRL-TK (Renilla luciferase) internal control vector (Promega) using Lipo6000 transfection reagent (Beyotime). After transfection for 48 h, cells were treated with CAP, and the luciferase activity was assayed using a Dual-Luciferase Reporter Assay System (Promega) according to the manufacture's instruction. The firefly signals were normalized against Renilla luciferase activity.

Colony formation assay

Colony formation assay was performed according to the previous reported protocols with some modifications (Xu et al., 2020b). In brief, 8505C cells were treated with CAP for 6 h, and then the cells were harvested, seeded into 24-well plates at a density of 1000 cells per well, and cultured overnight. Subsequently, the cells were incubated with 0.925 MBq carrier-free Na^{131}I for another 24 h. After being cultured for another 14 days, the colonies were fixed with methanol and stained with 0.02% (*w/v*) crystal violet for 15 min at RT. The visible colonies were photographed by a Cannon camera. For quantitative analysis, the crystal violet was dissolved by 33% glacial acetic acid and the optical absorbance were detected by a microplate reader at 570 nm (Epoch, Biotek).

Statistical analysis

All of the experiments were performed at least three times ($n = 3$) and the data were presented as mean ± SEM. Statistical analysis for IHC staining scores was practiced using Mann–Whitney U test. Significant difference was determined by Student's *t*-test for comparing two groups. Comparisons between three or more groups were conducted using a one-way analysis of variance (ANOVA), followed by Dunnett's *post hoc* test if ANOVA was significant ($P < 0.05$). *$P < 0.05$, significant difference; **$P < 0.01$, highly significant difference; ***$P < 0.001$, extremely significant difference. All the statistical analyses were conducted by GraphPad Prism 8.0 software.

Supplementary material

Supplementary material is available at *Journal of Molecular Cell Biology* online.

Conflict of interest: none declared.

References

Altarejos, J.Y., and Montminy, M. (2011). CREB and the CRTC co-activators: sensors for hormonal and metabolic signals. Nat. Rev. Mol. Cell Biol. *12*, 141–151.

Ben Abdelkhalek, M., Breton, M.F., Feliers, D., et al. (1994). TSH action on cAMP binding to the regulatory subunits of cAMP-dependent protein kinases in pig thyroid cell cultures. Mol. Cell. Endocrinol. *99*, 103–110.

Bible, K.C., Kebebew, E., Brierley, J., et al. (2021). 2021 American Thyroid Association guidelines for management of patients with anaplastic thyroid cancer. Thyroid *31*, 337–386.

Bolstad, B.M., Irizarry, R.A., Astrand, M., et al. (2003). A comparison of normalization methods for high density oligonucleotide array data based on variance and bias. Bioinformatics *19*, 185–193.

Buffet, C., Wassermann, J., Hecht, F., et al. (2020). Redifferentiation of radioiodine-refractory thyroid cancers. Endocr. Relat. Cancer *27*, R113–R132.

Cameron, E.G., and Kapiloff, M.S. (2017). Intracellular compartmentation of cAMP promotes neuroprotection and regeneration of CNS neurons. Neural Regen. Res. *12*, 201–202.

Caterina, M.J., Schumacher, M.A., Tominaga, M., et al. (1997). The capsaicin receptor: a heat-activated ion channel in the pain pathway. Nature *389*, 816–824.

Cheng, W., Liu, R., Zhu, G., et al. (2016). Robust thyroid gene expression and radioiodine uptake induced by simultaneous suppression of BRAF V600E and histone deacetylase in thyroid cancer cells. J. Clin. Endocrinol. Metab. *101*, 962–971.

Christophe-Hobertus, C., Lefort, A., Libert, F., et al. (2012). Functional inactivation of thyroid transcription factor-1 in PCCl3 thyroid cells. Mol. Cell. Endocrinol. *358*, 36–45.

Clark, R., and Lee, S.H. (2016). Anticancer properties of capsaicin against human cancer. Anticancer Res. *36*, 837–843.

Davies, T.F., Ando, T., Lin, R.Y., et al. (2005). Thyrotropin receptor-associated diseases: from adenomata to Graves disease. J. Clin. Invest. *115*, 1972–1983.

Di Benedetto, G., Scalzotto, E., Mongillo, M., et al. (2013). Mitochondrial Ca^{2+} uptake induces cyclic AMP generation in the matrix and modulates organelle ATP levels. Cell Metab. *17*, 965–975.

Diaz-Laviada, I., and Rodriguez-Henche, N. (2014). The potential antitumor effects of capsaicin. Prog. Drug Res. *68*, 181–208.

Dohan, O., De la Vieja, A., Paroder, V., et al. (2003). The sodium/iodide symporter (NIS): characterization, regulation, and medical significance. Endocr. Rev. *24*, 48–77.

Dunn, L.A., Sherman, E.J., Baxi, S.S., et al. (2019). Vemurafenib redifferentiation of BRAF mutant, RAI-refractory thyroid cancers. J. Clin. Endocrinol. Metab. *104*, 1417–1428.

Fast, S., Bonnema, S.J., and Hegedus, L. (2011). Radioiodine therapy of benign non-toxic goitre. Potential role of recombinant human TSH. Ann. Endocrinol. *72*, 129–135.

Fernández, L.P., López-Márquez, A., and Santisteban, P. (2015). Thyroid transcription factors in development, differentiation and disease. Nat. Rev. Endocrinol. *11*, 29–42.

Gancedo, J.M. (2013). Biological roles of cAMP: variations on a theme in the different kingdoms of life. Biol. Rev. Camb. Philos. Soc. *88*, 645–668.

Gao, L., Lin, Y., Jiang, Y., et al. (2019). Ultrasound characteristics of cervical lesions in patients with radioiodine refractory differentiated thyroid cancer: a strobe-compliant article. Medicine *98*, e17876.

Handkiewicz-Junak, D., Swierniak, M., Rusinek, D., et al. (2016). Gene signature of the post-Chernobyl papillary thyroid cancer. Eur. J. Nucl. Med. Mol. Imaging *43*, 1267–1277.

Hou, P., Bojdani, E., and Xing, M. (2010). Induction of thyroid gene expression and radioiodine uptake in thyroid cancer cells by targeting major signaling pathways. J. Clin. Endocrinol. Metab. *95*, 820–828.

Hwang, Y.P., Yun, H.J., Choi, J.H., et al. (2011). Suppression of EGF-induced tumor cell migration and matrix metalloproteinase-9 expression by capsaicin via the inhibition of EGFR-mediated FAK/Akt, PKC/Raf/ERK, p38 MAPK, and AP-1 signaling. Mol. Nutr. Food Res. *55*, 594–605.

Jiao, C., Li, L., Zhang, P., et al. (2020). REGgamma ablation impedes dedifferentiation of anaplastic thyroid carcinoma and accentuates radio-therapeutic response by regulating the Smad7–TGF-β pathway. Cell Death Differ. *27*, 497–508.

Josefsson, M., Evilevitch, L., Westrom, B., et al. (2006). Sodium–iodide symporter mediates iodide secretion in rat gastric mucosa in vitro. Exp. Biol. Med. *231*, 277–281.

Kambe, F., and Seo, H. (1997). Thyroid-specific transcription factors. Endocr. J. *44*, 775–784.

Kim, J., Gosnell, J.E., and Roman, S.A. (2020). Geographic influences in the global rise of thyroid cancer. Nat. Rev. Endocrinol. *16*, 17–29.

Kitaguchi, T., Oya, M., Wada, Y., et al. (2013). Extracellular calcium influx activates adenylate cyclase 1 and potentiates insulin secretion in MIN6 cells. Biochem. J. *450*, 365–373.

Kogai, T., Endo, T., Saito, T., et al. (1997). Regulation by thyroid-stimulating hormone of sodium/iodide symporter gene expression and protein levels in FRTL-5 cells. Endocrinology *138*, 2227–2232.

Landa, I., Ibrahimpasic, T., Boucai, L., et al. (2016). Genomic and transcriptomic hallmarks of poorly differentiated and anaplastic thyroid cancers. J. Clin. Invest. *126*, 1052–1066.

Lu, C.D., Altieri, D.C., and Tanigawa, N. (1998). Expression of a novel anti-apoptosis gene, survivin, correlated with tumor cell apoptosis and p53 accumulation in gastric carcinomas. Cancer Res. *58*, 1808–1812.

Luciani, P., Buci, L., Conforti, B., et al. (2003). Expression of cAMP response element-binding protein and sodium iodide symporter in benign non-functioning and malignant thyroid tumours. Eur. J. Endocrinol. *148*, 579–586.

Ma, M., Lin, B., Wang, M., et al. (2020). Immunotherapy in anaplastic thyroid cancer. Am. J. Transl. Res. *12*, 974–988.

Maniakas, A., Dadu, R., Busaidy, N.L., et al. (2020). Evaluation of overall survival in patients with anaplastic thyroid carcinoma, 2000–2019. JAMA Oncol. *6*, 1397–1404.

Martin, M., Modenutti, C.P., Peyret, V., et al. (2019). A carboxy-terminal monoleucine-based motif participates in the basolateral targeting of the Na^+/I^- symporter. Endocrinology *160*, 156–168.

Merritt, J.E., McCarthy, S.A., Davies, M.P., et al. (1990). Use of fluo-3 to measure cytosolic Ca^{2+} in platelets and neutrophils. Loading cells with the dye, calibration of traces, measurements in the presence of plasma, and buffering of cytosolic Ca^{2+}. Biochem. J. *269*, 513–519.

Nikiforov, Y.E., and Nikiforova, M.N. (2011). Molecular genetics and diagnosis of thyroid cancer. Nat. Rev. Endocrinol. *7*, 569–580.

Paz-Filho, G.J., and Graf, H. (2008). Recombinant human thyrotropin in the management of thyroid disorders. Expert Opin. Biol. Ther. *8*, 1721–1732.

Pita, J.M., Banito, A., Cavaco, B.M., et al. (2009). Gene expression profiling associated with the progression to poorly differentiated thyroid carcinomas. Br. J. Cancer *101*, 1782–1791.

Riedel, C., Levy, O., and Carrasco, N. (2001). Post-transcriptional regulation of the sodium/iodide symporter by thyrotropin. J. Biol. Chem. *276*, 21458–21463.

Saito, T., Endo, T., Kawaguchi, A., et al. (1997). Increased expression of the Na^+/I^- symporter in cultured human thyroid cells exposed to thyrotropin and in Graves' thyroid tissue. J. Clin. Endocrinol. Metab. *82*, 3331–3336.

Schmitt, J.M., Wayman, G.A., Nozaki, N., et al. (2004). Calcium activation of ERK mediated by calmodulin kinase I. J. Biol. Chem. *279*, 24064–24072.

Shang, H., Zhao, J., Yao, J., et al. (2020). Nevirapine increases sodium/iodide symporter-mediated radioiodide uptake by activation of TSHR/cAMP/CREB/PAX8 signaling pathway in dedifferentiated thyroid cancer. Front. Oncol. *10*, 404.

Silva, A.J., Kogan, J.H., Frankland, P.W., et al. (1998). CREB and memory. Annu. Rev. Neurosci. *21*, 127–148.

Smith, V.E., Franklyn, J.A., and McCabe, C.J. (2011). Expression and function of the novel proto-oncogene PBF in thyroid cancer: a new target for augmenting radioiodine uptake. J. Endocrinol. *210*, 157–163.

Subbiah, V., Kreitman, R.J., Wainberg, Z.A., et al. (2018). Dabrafenib and trametinib treatment in patients with locally advanced or metastatic BRAF V600-mutant anaplastic thyroid cancer. J. Clin. Oncol. *36*, 7–13.

Suzuki, K., Lavaroni, S., Mori, A., et al. (1998). Thyroid transcription factor 1 is calcium modulated and coordinately regulates genes involved in calcium homeostasis in C cells. Mol. Cell. Biol. *18*, 7410–7422.

Tanzarella, P., Ferretta, A., Barile, S.N., et al. (2019). Increased levels of cAMP by the calcium-dependent activation of soluble adenylyl cyclase in parkin-mutant fibroblasts. Cells *8*, 250.

Vassart, G., and Dumont, J.E. (1992). The thyrotropin receptor and the regulation of thyrocyte function and growth. Endocr. Rev. *13*, 596–611.

von Roemeling, C.A., Marlow, L.A., Pinkerton, A.B., et al. (2015). Aberrant lipid metabolism in anaplastic thyroid carcinoma reveals stearoyl CoA desaturase 1 as a novel therapeutic target. J. Clin. Endocrinol. Metab. *100*, E697–E709.

Wachter, S., Wunderlich, A., Greene, B.H., et al. (2018). Selumetinib activity in thyroid cancer cells: modulation of sodium iodide symporter and associated miRNAs. Int. J. Mol. Sci. *19*, 2077.

Wang, X.J., and Xu, J.X. (2005). Possible involvement of Ca^{2+} signaling in rotenone-induced apoptosis in human neuroblastoma SH-SY5Y cells. Neurosci. Lett. *376*, 127–132.

Weiss, S.J., Philp, N.J., and Grollman, E.F. (1984). Iodide transport in a continuous line of cultured cells from rat thyroid. Endocrinology *114*, 1090–1098.

Wojtas, B., Pfeifer, A., Oczko-Wojciechowska, M., et al. (2017). Gene expression (mRNA) markers for differentiating between malignant and benign follicular thyroid tumours. Int. J. Mol. Sci. *18*, 1184.

Xing, M. (2005). BRAF mutation in thyroid cancer. Endocr. Relat. Cancer *12*, 245–262.

Xing, M. (2013). Molecular pathogenesis and mechanisms of thyroid cancer. Nat. Rev. Cancer *13*, 184–199.

Xu, S., Cheng, X., Wu, L., et al. (2020a). Capsaicin induces mitochondrial dysfunction and apoptosis in anaplastic thyroid carcinoma cells via TRPV1-mediated mitochondrial calcium overload. Cell. Signal. *75*, 109733.

Xu, S., Pan, J., Cheng, X., et al. (2020b). Diallyl trisulfide, a H_2S donor, inhibits cell growth of human papillary thyroid carcinoma KTC-1 cells through a positive feedback loop between H_2S and cystathionine-gamma-lyase. Phytother. Res. *34*, 1154–1165.

Xu, S., Zhang, L., Cheng, X., et al. (2018). Capsaicin inhibits the metastasis of human papillary thyroid carcinoma BCPAP cells through the modulation of the TRPV1 channel. Food Funct. *9*, 344–354.

Yu, X.M., Jaskula-Sztul, R., Ahmed, K., et al. (2013). Resveratrol induces differentiation markers expression in anaplastic thyroid carcinoma via activation of Notch1 signaling and suppresses cell growth. Mol. Cancer Ther. *12*, 1276–1287.

Zhang, H., and Chen, D. (2018). Synergistic inhibition of MEK/ERK and BRAF V600E with PD98059 and PLX4032 induces sodium/iodide symporter (NIS) expression and radioiodine uptake in BRAF mutated papillary thyroid cancer cells. Thyroid Res. *11*, 13.

Zhong, T., Pan, X., Wang, J., et al. (2019). The regulatory roles of calcium channels in tumors. Biochem. Pharmacol. *169*, 113603.

Zhu, X., Enomoto, K., Zhao, L., et al. (2017). Bromodomain and extraterminal protein inhibitor JQ1 suppresses thyroid tumor growth in a mouse model. Clin. Cancer Res. *23*, 430–440.